Range of Photoparticle Recoil Atoms in Solids*

V. A. J. VAN LINT, M. E. WYATT, R. A. SCHMITT, C. S. SUFFREDINI, AND D. K. NICHOLS
General Atomic Division of General Dynamics Corporation, John Jay Hopkins Laboratory for Pure and Applied Science, San Diego, California

(Received 9 April 1965; revised manuscript received 30 July 1965)

The ranges of atoms recoiling from photonuclear reactions in various elements have been measured, utilizing foil-sandwich irradiations followed by standard radiochemical detection techniques. Different energy spectra of recoil atoms were achieved by varying the bremsstrahlung energy and the angle of emission relative to the incident photons. The results have been compared with some theoretical calculations. An empirical best fit to the data, using the reduced vector range and energy, ρ_V and ϵ, given by Lindhard, is $\rho_V = 2.4\epsilon^{0.74}$ for $\epsilon < 0.15$.

1. INTRODUCTION

THE passage of atomic particles through matter is of considerable interest, since a knowledge of the mechanisms involved in the slowing down of the energetic particles gives information about the particles and the medium through which they travel. The ranges measured in the present experiment are a test of the interatomic potentials used in theoretical calculations of the slowing down of particles in matter. Crystalline effects, which can have a pronounced influence on other experiments, should be of little importance in this case as the recoil atom starts from a lattice position in the foil and initially sees no open channels. Thus, the results are more directly comparable to theoretical models which assume a random solid. Domeij *et al.*,[1] measured the range of atoms on a metal foil having an anodically formed oxide layer. Using radiochemical techniques, the transmission was measured by counting the sample before and after removing the oxide layer. All other work as been done with gases as the stopping material, as by Lassen *et al.*,[2] or with crystalline solids.

In the present work, the range of atoms recoiling from (γ,n), (γ,p), and (γ,α) reactions has been measured by observing the fraction of resultant radioactive atoms which recoil out of a target foil into an adjacent catcher foil. Previous work performed at General Atomic by Schmitt and Sharp[3] and by van Lint *et al.*,[4] has been re-evaluated using a first approximation to a thick target bremsstrahlung and by including the recoil-atom energy spectra in the average range calculation instead of using an average value. Also, new data have been taken with (γ,p) and (γ,α) reactions to achieve higher energy recoils.

A sandwich of foils was constructed in which target foils were inserted between aluminum catcher foils. The sandwich was irradiated with bremsstrahlung produced by passing the electron beam from the General Atomic electron linear accelerator (Linac) through a 0.010-in.-platinum converter foil. Two orientations were used; in one the beam was normal to the plane of the foils, and in the other it was at an angle of 15 deg to the plane of the foils.

Nuclear reactions, resulting from absorption of bremsstrahlung gamma rays from the converter foil by the target foils and inelastic scattering of electrons in the target foils, produce recoil atoms which may escape from the target foils and imbed themselves in the catcher foils. If the recoil atoms were emitted isotropically and with a range R which was unique, a simple geometrical argument shows that the fraction f which recoils out of one surface of a target foil of thickness t would be

$$f = R/4t, \quad \text{for} \quad t \gg R. \tag{1}$$

In practice, there are two deviations from this simple picture: there is an appreciable spectrum of ranges due to the spectrum of energies of particles from the nuclear reactions; and the initial recoil energy is not isotropic, but is correlated with its initial direction of motion via the momentum imparted by the absorbed photon. The problems presented by these deviations are discussed in Secs. 2, 3, and 4.

The measurement of the fraction of atoms which recoil out of the target foils was performed by counting, with conventional radiochemical counting techniques, the activities of the catcher and target foils in identical geometry. Recoils which decayed by positron emission, where the 0.511-MeV annihilation radiation could be scintillation-counted, or beta decays with a prominent associated gamma ray were favored. Beta-minus counting was avoided to minimize corrections for self-absorption and back-scattering in the sample.

2. GAMMA-RAY ABSORPTION

Electrons from the Linac are monoenergetic within 5%, the average energy being dependent on the strength of the current in a deflection magnet. These electrons transverse a converter and a target sandwich producing photons. The incident photon spectrum was assumed to

* This research was supported in part by Aeronautical Research Laboratories and by the Office of Aerospace Research, under Contract AF33(616)-6795.

[1] B. Domeij *et al.*, Can. J. Phys. **42**, 1624 (1964).

[2] N. O. Lassen *et al.*, paper presented at the Conference on the Physics of the Electromagnetic Separation Method, Paris, 1962 (unpublished).

[3] R. A. Schmitt and R. A. Sharp, Phys. Rev. Letters **1**, 445 (1958).

[4] V. A. J. van Lint, R. A. Schmitt, and C. S. Suffredini, Phys. Rev. **121**, 1457 (1961).

consist of three parts: one due to the bremsstrahlung produced in the 0.010-in. platinum converter and in those materials in the sandwich holder upstream from the target foil; another due to the bremsstrahlung produced in the target foil itself; and lastly, one due to the virtual bremsstrahlung spectra produced by inelastic electron scattering on the nuclei of the target foil.

When the electron energy is near or below the maximum of the (γ,n) cross section, the softening of the photon spectrum, due to the thickness of the converter used, can have a measurable effect on the evaporated nucleon spectra. Thus, a first approximation to a thick-target bremsstrahlung spectrum was used where the average energy loss of the electrons was taken into account, but where energy-straggling or multiple-scattering was neglected. A Schiff spectrum, as evaluated by Penfold and Leiss,[5] was assumed for each thickness Δt of the converter, Δt corresponding to an average energy loss of 0.2 MeV for electrons of the average energy incident on that thickness element. Thus, the incident photon spectrum due to bremsstrahlung produced in materials upstream of the target foils is

$$\Psi=\sum_{i=0}^{n}\frac{\eta_c(E_i)}{\eta_{\mathrm{Pt}}(E_i)}\Delta E\frac{\varphi(E_i,k)}{k}, \tag{2}$$

where η_{Pt} and η_c, respectively, are the radiation efficiencies (or the fraction of the total energy loss that produces bremsstrahlung) of the platinum and other converter materials, $\varphi(E_i,k)$ is the bremsstrahlung intensity spectrum, from Penhold and Leiss,[5] for electrons of energy E_i in platinum, k is the gamma energy, ΔE is the average energy loss of electrons in Δt_i (i.e., 0.2 MeV), E_0 is the Linac energy, $E_{i+1}=E_i-0.2$ MeV, and the summation extends through all converter materials.

For the target materials, η_c is modified to

$$\eta_c(E_i)\,|_{\mathrm{target}}=\eta_c(E_i)[r(\Delta t_i/t)+(t-\sum_{j=0}^{i}\Delta t_j)/t], \tag{3}$$

where the first term in the brackets is the contribution due to virtual bremsstrahlung associated with inelastic electron scattering on the target nuclei, and the second is the effect of internally produced bremsstrahlung on subsequent Δt's. In Δt_i, the relative activations r due to electrons and bremsstrahlung is given by[6]

$$r=\Delta t_i\rho(N_0/A)FZ(Z+1)r_0^2, \tag{4}$$

where ρ is the density, A and Z are the atomic weight and number, N_0 is Avogadro's number, F is an experimentally derived constant ~ 8, and r_0 is the classical electron radius.

The photon spectrum calculated on a computer by the above process was used as the incident photon spectrum to calculate the neutron spectrum from (γ,n) reactions by the method described in the following sections.

3. PHOTOPARTICLE SPECTRA

Photoneutron spectra are treated from the standpoint of resonance direct[7] and evaporation theory,[8] assuming isotropic emission in the center-of-mass (c.m.) system with a spectrum given by[9]

$$F(E_n)dE_n=K\int_{E_t+E_n}^{E_0}dk\,\sigma_{\gamma,n}(k)\Psi(k)$$
$$\times\Bigg(\Big(E_n\exp\{2[\alpha(k-E_t-E_n]^{1/2}\}\Big/\int_0^{k-E_t}dx\,x$$
$$\times\exp\{2[\alpha(k-E_t-x)]^{1/2}\}\Big)$$
$$+\frac{b}{\min(E_c,E_n)}[u(k-E_t-E_n)-u(k-E_t)]\Bigg)dE_n, \tag{5}$$

where $F(E_n)$ is the neutron-energy distribution function, E_n is the neutron energy, K is a normalization constant, E_0 is the peak bremsstrahlung energy, E_t is the gamma energy at the photoneutron threshold, $\sigma_{x,n}(k)$ is the experimental photoneutron cross section, Ψ is the incident photon spectrum from Sec. 2, α is the level density parameter taken from experimental evidence[10,11] [or assumed to be $A/(10\ \mathrm{MeV})$, where A is the mass of the product nucleus], b is the fraction of resonance direct particles, $\min(E_c,E_n)$ is the minimum value of E_c and E_n, E_c is a constant assumed to be 8 MeV, and the $u(a)$ are unit step functions $u(x)=0$, $x<a$; $u(x)=1$, $x>a$.

In Eq. (5), the first term represents the evaporation neutron spectrum using a level density of the form

$$\omega(E^*)=\mathrm{const}\exp[2(\alpha E^*)^{1/2}], \tag{6}$$

where E^* is the excitation energy of the residual nucleus. The second term is the contribution from the directly ejected neutrons leaving the residual nucleus with equal probability in states from the ground state to E_c below the ground state.

A more rigorous treatment of the nuclear Fermi-gas model by Ericson[12] gives a level density expression of the form

$$\omega(E^*)=(\mathrm{const}/E^{*2})\exp[2(a'E^*)^{1/2}], \tag{7}$$

but experiment[10] shows an excess of higher energy ejected neutrons over either level density expression, and it is just this region where the two expressions differ

[5] A. S. Penfold and J. F. Leiss, University of Illinois Report (unpublished).
[6] K. L. Brown, Phys. Rev. **93**, 443 (1954).
[7] D. H. Wilkinson, Physica **22**, 1039 (1956).
[8] V. F. Weisskopf and D. H. Ewing, Phys. Rev. **57**, 472 (1940).
[9] G. Cortini *et al.*, Nuovo Cimento **14**, 54 (1959).
[10] D. G. Thompson, Phys. Rev. **129**, 1649 (1963).
[11] E. Erba, Nuovo Cimento **22**, 1237 (1961).
[12] T. Ericson, Advan. Phys. **9**, 425 (1960).

most and where the calculations for the directly ejected neutron component is expected to dominate. A further complication in the choice of a level density expression is the fact that some nuclei are best explained by nuclear melting, with a level density proportional to $\exp(E^*/T)$, where T is the nuclear temperature. Thus it was felt that the choice of the evaporation spectrum given in Eq. (5) was justified, since the different expressions give similar shapes at the average neutron energy, and the high-energy side must be accounted for by other means. The level density parameters used were those derived from inelastic neutron scattering[10,11,13] at about 6 MeV, which is the approximate difference between the peak of the giant resonance and the (γ,n) threshold. When experimental data were not available, systematics were followed which take shell effects into account.[14] The resonance direct spectrum with constant b assumes that the cross section for direct ejection is proportional to the total (γ,n) cross section. Even if this assumption were invalid in the heavier nuclei, the term represents only a small correction, and its magnitude is adjusted to force agreement between the theoretical spectrum and measurements.

Experimental spectra were used for proton and alpha photoparticles. Where spectra for a particular reaction had not been measured, spectra from neighboring elements were used, since the main factor affecting the charged photoparticle spectra peaks is the Coulomb barrier. Also, spectra summed over all angles were used. The effects of these procedures are discussed in the following section.

4. RECOIL NUCLEI

In the present experiments, the recoil nuclei are uniformly generated throughout the target foil thickness, but they are not isotropically emitted because of the momentum contributed by the absorbed gamma rays. Furthermore, because of the large variation in the energies of the absorbed gamma rays and emitted neutrons, the range spectrum is very broad. These effects must be considered in computing the fraction of the atoms which recoil out of the target foils.

It has been shown[4] that for the absorption of a monoenergetic gamma ray of energy k, followed by emission of a monoenergetic nucleon at momentum P_n, the fraction f_ω of the atoms recoiling out of a foil of thickness t, which is oriented with its normal at an angle ω to the gamma ray, is to second order in $\eta=k/P_n$,[15]

$$f_{0°,180°}=\frac{R_0}{4t}(1\pm\tfrac{4}{3}\eta+\tfrac{1}{4}\eta^2)+\frac{P_n}{4t}\frac{dR}{dP}(\pm\tfrac{2}{3}\eta+\tfrac{3}{4}\eta^2), \quad (8)$$

$$f_{90°}=\frac{R_0}{4t}(1-\eta^2/8)+\frac{P_n}{32t}\frac{dR}{dP}\eta^2, \quad (9)$$

where the range at any momentum can be adequately described by a first-order Taylor expansion about P_n,

$$R(P)=R_0(P_n)+(dR/dP)_{P=P_n}(P-P_n). \quad (10)$$

From analysis of previous data,[2] it was found that an expression of the form $R=BP^\beta$ satisfied the data over a wide range. Inserting this into the above formula for the recoil fraction gives

$$f_{0°,180°}=\frac{B}{4t}P_n{}^\beta[1\pm\tfrac{4}{3}\eta+\tfrac{1}{4}\eta^2+\beta(\pm\tfrac{2}{3}\eta+\tfrac{3}{4}\eta^2)], \quad (11)$$

$$f_{90°}=\frac{B}{4t}P_n{}^\beta(1-\tfrac{1}{8}\eta^2+\tfrac{1}{8}\beta\eta^2). \quad (12)$$

To the same order of approximation, the momenta may be expressed as

$$P_{0°,180°}=P_n[1\pm\tfrac{2}{3}\eta-(5/36)\eta^2], \quad (13)$$

$$P_{90°}=P_n(1+\tfrac{1}{8}\eta^2). \quad (14)$$

In the general case, when both the gamma and nucleon energies are distributed, the recoil fraction should be computed by integration over these distributions. This was done for the nucleon energy distribution $F(E_n)$, where $\bar{f}_\omega$ and $\bar{P}_\omega$, the average values of f_ω and P_ω, were taken over $F(E_n)$. The average value of the absorbed photon energy $\bar{k}$ was used, however. This is justified by considering the shape of the absorbed photon spectra. Due to the giant resonance shape which has a peak around 20 MeV and a half-width of a few MeV,

$$k^2=(\bar{k}+\Delta k)^2\approx\bar{k}^2(1+\Delta k/k), \quad (15)$$

where $\Delta k/k$ is of the order of a tenth, giving a small correction to a second-order term which is itself small.

5. EXPERIMENTAL DETAILS

Because impurities on the surface of the foils could affect the measurements, before being assembled into sandwiches the foils were thoroughly cleaned by a degreasing rinse, an acid etch when possible, and a final rinse in conductivity water. A typical sandwich was then assembled from the following components: 20 target foils of the order of 0.001-in. thick, each one between two 0.0012-in. aluminum catchers; a packet of 20 aluminum foils, prepared exactly as the catcher foils, to serve as background monitors; two copper monitor foils placed on the front and back of the foil sandwich

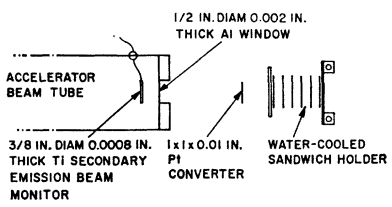

FIG. 1. Irradiation geometry.

[13] D. W. Lang, Nucl. Phys. **26**, 434 (1961).
[14] T. D. Newton, Can. J. Phys. **34**, 804 (1956).
[15] Units are chosen so that the velocity of light is unity.

TABLE I. Counting and reference data.

Target	Product		Radiation counted	Detector[a]	Sample[b]	Cross section reference	Spectra reference
Ti^{46}	3.08-h	Ti^{45}	0.511 MeV γ (β^+)	scin.	foil	c	
Ti^{48}	3.4-day	Sc^{47}	0.160 MeV γ	scin.	foil	c	aa
Ti^{49}	44-h	Sc^{48}	0.820 MeV γ	scin.	foil	c	aa
V^{51}	3.4-day	Sc^{47}	0.160 MeV γ	PHA	foil	d	bb
Cr^{50}	42-min	Cr^{49}	0.511 MeV γ (β^+)	scin.	HCl sol.	e	
Fe^{54}	9-min	Fe^{53}	0.511 MeV γ (β^+)	scin.	foil	f	
Fe^{57}	2.58-h	Mn^{56}	0.85 MeV γ	scin.	foil	g	cc
Ni^{58}	36-h	Ni^{57}	1.38 MeV γ	scin.	foil	h	
Ni^{62}	1.65-h	Co^{61}	0.070 MeV γ	scin.	foil	h	dd, ee
Cu^{63}	9.9-min	Cu^{62}	0.511 MeV γ (β^+)	scin.	foil	i	
Cu^{65}	12.8-h	Cu^{64}	0.511 MeV γ (β^+)	scin.	foil	i	
Cu^{65}	1.65-h	Co^{61}	0.070 MeV γ	scin.	HNO_3 sol.	j	ff
Zn^{68}	61-h	Cu^{67}	0.180 MeV γ	scin.	Cu SCN ppt.	k	k
Ge^{70}	40-h	Ge^{69}	0.511 MeV γ (β^+)	scin.	CP-4 sol.	l	
Zr^{90}	4.4-min	Zr^{89m}	0.59 MeV γ	scin.	foil	m	
Zr^{90}	79-h	Zr^{89}	0.91 MeV γ	scin.	foil	m	
Zr^{91}	64-h	Y^{90}	β^-	LBBC	$Y_2(C_2O_4)_3$ $\times 10$ H_2O ppt.	n	gg, hh, ii
Zr^{91}	2.8-h	Sr^{87}	0.390 MeV γ	PHA	foil	o	jj
Zr^{94}	10-h	Y^{93}	β^-	LBBC	$Y_2(C_2O_4)_3$ $\times 10$ H_2O ppt.	n	gg, hh, ii
Mo^{92}	15.6-min	Mo^{91}	0.511 MeV γ (β^+)	scin.	foil	p	
Mo^{100}	67-h	Mo^{99}	>0.070 MeV γ	scin.	foil	n	
Rh^{103}	220-day	Rh^{102}	0.511 MeV γ (β^+)	scin.	foil	q	
Pd^{110}	13.6-h	Pd^{109}	0.088 MeV γ	scin.	foil	q	
Ag^{107}	8.3-day	Ag^{106}	0.51 MeV γ	scin.	foil	q	
Ag^{107}	24-min	Ag^{106m}	0.511 MeV γ (β^+)	scin.	foil	q	
Cd^{106}	55-min	Cd^{105}	0.511 MeV γ (β^+)	scin.	foil	q	
Cd^{112}	7.5-day	Ag^{111}	β^-	LBBC	Ag Cl ppt.	r	kk, ii
Cd^{113}	3.12-h	Ag^{112}	β^-	LBBC	Ag Cl ppt.	r	kk, ii
Cd^{114}	5.3-h	Ag^{113}	β^-	LBBC	Ag Cl ppt.	r	kk, ii
Cd^{116}	54-h	Cd^{115}	0.340 MeV γ	scin.	foil	q	
Cd^{116}	43-day	Cd^{115m}	β^-	LBBC	Cd NH_4 PO_4 ppt.	q	
Sn^{124}	40-min	Sn^{123}	0.150 MeV γ	scin.	foil	s	
Gd^{160}	18-h	Gd^{159}	0.360 MeV γ	scin.	foil	t	
Ta^{181}	8.1-h	Ta^{180m}	0.065 MeV γ	PHA	foil	u	
Au^{197}	6.1-day	Au^{196}	0.35 MeV γ	scin.	foil	v	
Th^{232}	25-h	Th^{231}	40–110 keV γ	scin.	foil	w	

[a] Scin. is the crystal spectrometer described in Ref. 2, PHA is the same with a 256-channel pulse-height analyzer, and LBBC is a low-background proportional beta counter.

[b] All gamma counting was done in the geometry of Ref. 2. Foils were counted directly. After chemical purification, a precipitate was counted on filter paper or a solution was counted in a 2-dram polyvial placed in the foil position.

[c] T. R. Sherwood and W. E. Turchinetz, Nucl. Phys. **29**, 292 (1962).
[d] J. H. Carver, Proc. Phys. Soc. (London) **77**, 417 (1961).
[e] J. Goldemberg and L. Katz, Can. J. Phys. **32**, 49 (1954).
[f] L. Katz *et al.*, Phys. Rev. **82**, 271(L) (1951).
[g] J. Halpern and A. K. Mann, Phys. Rev. **83**, 370 (1951).
[h] J. H. Carver and W. Turchinetz, Proc. Phys. Soc. (London) **A73**, 585 (1959).
[i] S. C. Fultz *et al.*, Phys. Rev. **133**, B1149 (1964).
[j] R. N. H. Haslam *et al.*, Phys. Rev. **84**, 840(L) (1951).
[k] N. V. Linkova *et al.*, Zh. Eksperim. i Teor. Fiz. **38**, 780 (1960) [English transl.: Soviet Phys.—JETP **11**, 566 (1960)].
[l] O. A. Borello *et al.*, Ann. acad. brasil. si. **27**, 413 (1955).
[m] R. Nathans and P. F. Yergin, Phys. Rev. **98**, 1296 (1955).
[n] F. Ferrero *et al.*, Nuovo Cimento **6**, 585 (1957).
[o] R. N. H. Haslam and H. M. Skarsgard, Phys. Rev. **81**, 497(L) (1951).
[p] N. Mutsuro *et al.*, J. Phys. Soc. Japan **14**, 1649 (1959).
[q] O. V. Bogdankevich *et al.*, Zh. Eksperim. i Teor. Fiz. **42**, 1502 (1962) [English transl.: Soviet Phys.—JETP **15**, 1044 (1962)].
[r] Kuo Chi-ti and B. S. Ratner, Zh. Eksperim. i Teor. Fiz. **39**, 1578 (1960) [English transl.: Soviet Phys.—JETP **12**, 1098 (1960)].
[s] Kuo Chi-ti *et al.*, Zh. Eksperim. i Teor. Fiz. **40**, 85 (1961) [English transl.: Sovit Phys.—JETP **13**, 60 (1961)].
[t] R. L. Bramblett *et al.*, Phys. Rev. **133**, B869 (1964).
[u] R. L. Bramblett *et al.*, Phys. Rev. **129**, 2723 (1963).
[v] S. C. Fultz *et al.*, Phys. Rev. **127**, 1273 (1962).
[w] L. Katz *et al.*, Can. J. Phys. **35**, 470 (1957).
[aa] A. P. Komar and T. N. Drugnev, Dokl. Akad. Nauk SSSR **126**, 1234 (1959) [English transl.: Soviet Phys.—Doklady **4**, 653 (1959)].
[bb] M. Kregar and B. Povh, Phys. Letters **2**, 103 (1962).
[cc] M. E. Toms and W. E. Stephens, Phys. Rev. **95**, 1209 (1954).
[dd] E. M. Lejkin *et al.*, Nuovo Cimento **3**, Suppl. 1, 105 (1956).
[ee] B. M. Spicer *et al.*, Australian J. Phys. **10**, 217 (1957).
[ff] M. Kregar and B. Povh, Nucl. Phys. **43**, 170 (1963).
[gg] R. M. Osokina, Zh. Eksperim. i Teor. Fiz. **44**, 444 (1963) [English transl.: Soviet Phys.—JETP **17**, 303 (1963)].
[hh] W. A. Butler and G. M. Aleny, Phys. Rev. **91**, 58 (1953).
[ii] W. C. Barker and V. J. Vanhuyse, Nucl. Phys. **16**, 381 (1960).
[jj] P. Erdös *et al.*, Helv. Phys. Acta **30**, 639 (1957).
[kk] M. E. Toms and W. E. Stephens, Phys. Rev. **92**, 362 (1953).

(the 12.8-h-Cu^{64} activity in these foils was used to measure the integrated gamma exposure of the sandwich); one aluminum clamping plate with $\frac{1}{16}$-in.-thick center section, provided with water cooling around its periphery: and one $\frac{1}{16}$-in.-thick aluminum clamping plate.

The irradiation geometry used is illustrated in Fig. 1. The irradiations usually lasted 20 min. with an aver-

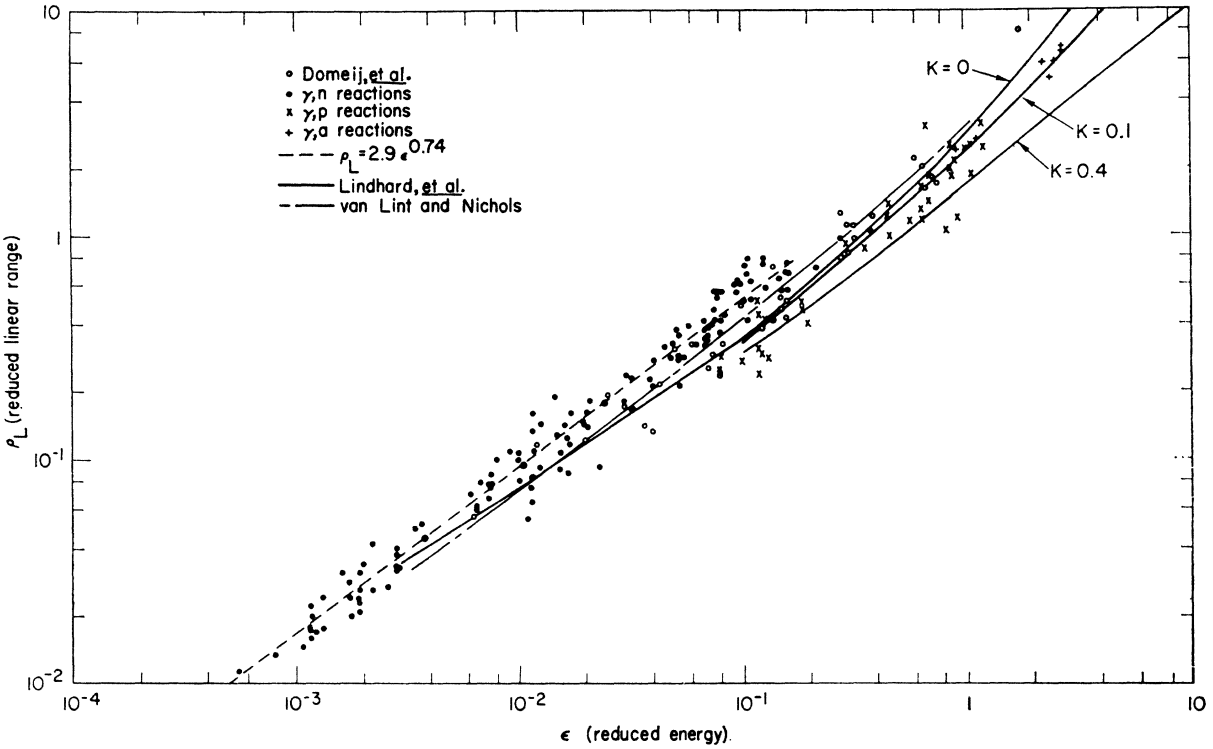

FIG. 2. Comparison of range-energy data with theoretical predictions.

age gamma exposure rate of the order of 10^5 rad/min. After irradiation, the sandwiches were disassembled and mounted on $\frac{1}{16}$-in.-aluminum cards for scintillation counting. Individual samples for counting included all forward catchers, all backward catchers, all background monitors, the central target foil, and the two intensity monitors.

On some materials, where there were interfering activities, a chemical separation was performed before counting. Table I gives the radiation counted, the detection method used, and the material counted.

Various check experiments were performed. It has been established that less than 0.5% of the Cu^{62}, less than 1.6% of the Ag^{106m}, and less than 2.4% of the Au^{196} atoms incident on the aluminum catchers are reflected. Furthermore, by neutron activation analysis of the catchers, it has been shown that less than 0.3% of the activity on the catchers could be ascribed to material which may have rubbed off the target onto the catchers. It was further established by irradiation of sandwiches in vacuum that the presence of small amounts of air between the target and catcher foils has no effect on the range measurements, which were normally performed on tightly clamped sandwiches in normal atmosphere. For the case of Cu, it was shown by ion-bombardment cleaning of a foil in an argon atmosphere and immediate irradiation in vacuum that the surface oxide layer changed the recoil fraction by less than 5±10%. More details of the experimental procedure are given in a previous report.[4]

6. EXPERIMENTAL RESULTS

Figure 2 summarizes the results of the range measurements utilizing (γ,n), (γ,p), and (γ,α) reactions. The calculated average recoil energy is derived from the average recoil momentum $\bar{P}_\omega$ and corresponds to the average recoil energy in the particular direction. The measured range, $4tf$, has been multiplied by the factor $C_\omega = B\bar{P}_\omega\beta/4t\bar{f}_\omega$ to calculate the corrected ranges. At angles other than $\omega=0$ deg, 90 deg, and 180 deg, the calculation of $\bar{f}_\omega$ and $\bar{P}_\omega$ has not been performed, but an interpolation assuming the correction terms to be proportional to $\cos\omega$ was used. This interpolation has the proper value for the calculated angles and is sufficiently accurate when compared with the other assumptions. Angles of 0–180 deg are taken from earlier data and represent an average of 0 deg and 180 deg catchers.

The experimentally observable quantity corresponds to the vector range which is calculated as described in the Appendix of this paper, while the linear range is plotted in Fig. 2 to conform with theoretical treatments. The calculated value for the ratio of linear to vector range of 1.2 has been used to correct the data. The reduced linear range ρ_L and energy ϵ have been plotted with

$$\rho_L = 1.2RN\pi\lambda^2[4M_RM_L/(M_R+M_L)^2], \quad (16)$$

$$\epsilon = E(\lambda/e_0^2Z_RZ_L)(M_L/M_R+M_L), \quad (17)$$

where M_R and M_L are the masses of the recoil and lattice atom, respectively, R is the corrected range, E is

the calculated recoil energy, N is the atom density, e_0 is the electronic charge, and

$$\lambda = 0.8853 a_0 (Z_R^{2/3} + Z_L^{2/3})^{-1/2}, \quad (18)$$

where a_0 is the Bohr radius, and Z_R and Z_L are the atomic numbers of the recoil and lattice atom, respectively.

Sources of error in the range measurements are typically
- counting statistics 5%;
- approximations in derivation of corrected range 5%;
- thickness of target foils (derived from weight and area) 1%;
- reflection of recoil atoms from catcher foils <2%;
- correction for relative counting geometry (including absorption and backscattering between target and catcher foils) 4%.

Errors in average recoil energy are estimated to be
- for calibration of accelerator energy 3%;
- for calculation of neutron-energy spectrum 15%;
- for approximations in the formula for deriving average recoil energy 10%.

7. DISCUSSION

The photoneutron data are consistent with an empirical range-energy expression of the form $\rho_V = 2.4\epsilon^{0.74}$. The exponent $\beta = 0.74$ used in the reduction of the data is borne out very well by the forward and backward catcher pairs ($\omega = 0$ deg, 180 deg; 75 deg, 105 deg) from single irradiations; otherwise, there is much scatter between irradiations. Recoil fractions from identical irradiations differ by as much as 50% while keeping their forward and backward ratios consistent within a few percent of $\epsilon^{0.74}$. The sources of error given above cannot explain this discrepancy, but the number of data points is large enough to fix the scale factor for the range as 2.4 ± 0.3. Comparison with the theoretical curve of Lindhard *et al.*,[16] shows the data to have a steeper slope, with a crossing around a reduced energy of $\epsilon = 10^{-3}$. The data lie approximately 25% above the theoretical curve (van Lint and Nichols) using the Thomas-Fermi (TF) potential (see Appendix) throughout the range of the photoneutron data. The data of Domeij *et al.*,[1] tend to be below our data, also, and lie much closer to the curve of van Lint and Nichols. However, the slope of our data agrees quite well with other experimental evidence and theory.

The photo-alpha reaction data fall slightly above the theoretical predictions of Lindhard,[16] taking into account inelastic scattering with a value for K of 0.15 for the elements studied.

In general, the photo-proton reaction points lie below the theoretical curves and do not exhibit the forward and backward ratios assumed in the reduction of the recoil fraction to a range. This can be explained by the fact that the photo-protons were assumed to be emitted isotropically in the c.m. system. There is evidence that the high-energy protons are emitted preferentially near 90 deg, thus reducing the average recoil energy in the forward and backward direction.

APPENDIX

A Monte Carlo computer program has been developed to determine the range of atoms which move through a random lattice. The calculations assume that the energy loss of an atom occurs in a series of collisions with a single lattice atom (binary collisions) and that the scattering process can be described by classical mechanics. The program has been designed to use any interatomic potential, but the well-established Thomas-Fermi potential is considered here. Previous work on this problem by Lindhard, *et al.*,[16] assumed that the discrete scattering events could be treated as a continuous process. His analytical solution for the linear range has served as a basis for comparison with much experimental data, which measures the penetration of atoms along their initial direction, when his given correction factor is applied. Oen and Robinson[17] took into account the discrete nature of tne energy loss process, using a Monte Carlo program closely related to that outlined here, in which the linear range and the distribution of atoms along their initial direction of penetration are described. The theoretical work performed in conjunction with this experiment supplements the foregoing by providing a calculation of the vector range in order to reduce the data to Lindhard's units of linear range and energy.

The Monte Carlo program determines the histories of a large number of atoms on the assumption that each atom will pass through a certain number of discrete energy states. At each energy state, the atom will have a characteristic mean free path for an energy-transfer collision, which is a function of the atom's energy and of the value of the next-lowest discrete energy state. At the time of collision, each atom will also have a certain probability of entering each of many different lower energy states as calculated by evaluation of the classical scattering integral. The number of energy states is large enough so that larger energy-transfer events are accurately described by the finite number of energies available to the scattered atom and by the corresponding differential collision cross section. However, for the lowest

[16] J. Lindhard, M. Scharff, and H. E. Schiott, Kgl. Danske Videnskab. Selskab, Mat. Fys. Medd. 33, No. 14 (1963).

[17] Ordean S. Oen and Mark T. Robinson, J. Appl. Phys. 35, 2515 (1964).

energy transfers (and smallest angle of scattering) a special averaging of the energy loss is needed, because the single-atom collision cross section is unbounded. This problem is resolved by equating the energy loss to the next lower energy interval to an integral of the product of the energy loss and of the differential energy cross section. Thus, for the lowest energy transfers, the collision process is treated as continuous.

The output data from the program include the linear range, vector range, distance of penetration, straggling in vector range, rms scattering angle, and histories of a selected number of atoms.

PHYSICAL REVIEW VOLUME 147, NUMBER 1 8 JULY 1966

Critical Temperatures and Critical Fields of Multiple Superconducting and Normal-Conducting Films*†

R. J. DUFFY‡ AND HANS MEISSNER
Department of Physics, Stevens Institute of Technology, Hoboken, New Jersey
(Received 13 December 1965)

The critical temperatures and critical magnetic fields have been determined for a series of superposed normal and superconducting films. Both Cu-Sn and Au-Sn samples were investigated. The samples were prepared by vacuum-deposition methods or by electroplating. Thicknesses of the Sn films ranged from 160 to 2700 Å. The dependence of the critical temperature T_c of the multiple film on normal-metal thickness is compared with recent theories. Experimental evidence is given that the observed effects are true proximity effects, caused by the free exchange of electrons between the two metals, and that metallic diffusion alone is not responsible for the observed phenomena. The critical magnetic fields of both single and multiple films are compared with the microscopic theories. It is shown that at fields near the critical fields with the multiple film still superconducting the gap function $\Delta(\mathbf{r})$ and the magnetization are negligibly small on the normal side of the film.

I. INTRODUCTION

IF a thin specimen of a superconducting metal is in intimate contact with a normal conducting metal (or another superconductor which is still in the normal state at the temperature in question), the value of the critical temperature T_c is lower than the value for the superconductor alone. Many recent experiments[1–8] have investigated this phenomenon and several theoretical explanations have been proposed.[6,7,9–12] Werthamer[7,11] and de Gennes[12] have shown that such a proximity effect should exist because of a change in the gap function $\Delta(\mathbf{r})$. The value of $\Delta(\mathbf{r})$ is altered in the superconductor due to the presence of the normal metal and takes on a nonzero value in the normal side. The lowest eigenvalue of their equation for $\Delta(\mathbf{r})$ gives the value of T_c for each sample. In general $\Delta(\mathbf{r})$ is a function of the magnetic field and goes to zero at the critical magnetic field H_c. Since $\Delta(\mathbf{r})$ is altered by the presence of a normal metal, H_c also should vary as a function of the thickness of the normal metal.

In this paper we present our results of the determination of T_c and H_c (parallel to the film), for thin multiple film samples. Our samples were made by vacuum deposition of the metals on glass substrates. Resistance measurements were used to determine H_c as a function of temperature. To obtain meaningful data in this way, it was necessary to mechanically trim the sample edges, assuring a constant film thickness. Thus each sample was at room temperature for a short time, causing some unavoidable diffusion between the two metals.

In Sec. II we present the experimental procedures used for fabricating the samples and for determining the resistance, T_c, and H_c of each sample. Section III discusses the resistances of each set of samples showing the effects of diffusion. In Sec. IV we present the data for T_c and show the effects of diffusion and of the proximity of the normal metal on the value of T_c. Section V then treats H_c both for single and composite films. The results

* Based on a thesis submitted to the Department of Physics of Stevens Institute of Technology in partial fulfillment of the requirements for the Ph.D. degree.

† Supported in part by the National Aeronautics and Space Administration.

‡ Present address: National Bureau of Standards, Institute for Materials Research, Boulder, Colorado.

[1] H. Meissner Phys. Rev. **117**, 672 (1960); IBM J. Res. Develop. **6**, 71 (1962).
[2] H. Meissner, in *Proceedings of the 8th International Conference on Low Temperature Physics* (Butterworth, Inc., Washington, D. C., 1964), p. 365.
[3] P. H. Smith, S. Shapiro, T. L. Miles, and J. Nicol, Phys. Rev. Letters **6**, 686 (1961).
[4] W. A. Simmons and D. H. Douglass, Jr., Phys. Rev. Letters **9**, 153 (1962).
[5] P. Hilsch, Z. Physik **167**, 511 (1962).
[6] P. Hilsch and R. Hilsch, Z. Physik **180**, 10 (1964).
[7] J. J. Hauser, H. C. Theurer, and N. R. Werthamer, Phys. Rev. **136**, A637 (1964).
[8] J. J. Hauser and H. C. Theurer, Phys. Letters **14**, 270 (1965).
[9] L. N. Cooper, Phys. Rev. Letters **6**, 89 (1962).
[10] D. H. Douglass, Jr., Phys. Rev. Letters **9**, 155 (1962).
[11] N. R. Werthamer, Phys. Rev. **132**, 2440 (1963).
[12] P. G. de Gennes, Rev. Mod. Phys. **36**, 225 (1964).